



UNIVERSITY OF LEEDS

This is a repository copy of *Advanced biofilm staining techniques for TEM and SEM in geomicrobiology: Implications for visualizing EPS architecture, mineral nucleation, and microfossil generation.*

White Rose Research Online URL for this paper:  
<http://eprints.whiterose.ac.uk/137532/>

Version: Accepted Version

---

**Article:**

McCutcheon, J [orcid.org/0000-0002-9114-7408](https://orcid.org/0000-0002-9114-7408) and Southam, G (2018) Advanced biofilm staining techniques for TEM and SEM in geomicrobiology: Implications for visualizing EPS architecture, mineral nucleation, and microfossil generation. *Chemical Geology*, 498. pp. 115-127. ISSN 0009-2541

<https://doi.org/10.1016/j.chemgeo.2018.09.016>

---

© 2018 Elsevier B.V. This manuscript version is made available under the CC-BY-NC-ND 4.0 license <http://creativecommons.org/licenses/by-nc-nd/4.0/>.

**Reuse**

This article is distributed under the terms of the Creative Commons Attribution-NonCommercial-NoDerivs (CC BY-NC-ND) licence. This licence only allows you to download this work and share it with others as long as you credit the authors, but you can't change the article in any way or use it commercially. More information and the full terms of the licence here: <https://creativecommons.org/licenses/>

**Takedown**

If you consider content in White Rose Research Online to be in breach of UK law, please notify us by emailing [eprints@whiterose.ac.uk](mailto:eprints@whiterose.ac.uk) including the URL of the record and the reason for the withdrawal request.

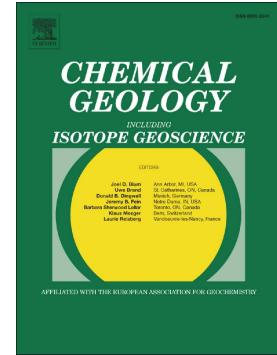


[eprints@whiterose.ac.uk](mailto:eprints@whiterose.ac.uk)  
<https://eprints.whiterose.ac.uk/>

# Accepted Manuscript

Advanced biofilm staining techniques for TEM and SEM in geomicrobiology: Implications for visualizing EPS architecture, mineral nucleation, and microfossil generation

Jenine McCutcheon, Gordon Southam



PII: S0009-2541(18)30456-X  
DOI: doi:[10.1016/j.chemgeo.2018.09.016](https://doi.org/10.1016/j.chemgeo.2018.09.016)  
Reference: CHEMGE 18909  
To appear in: *Chemical Geology*  
Received date: 30 April 2018  
Revised date: 23 August 2018  
Accepted date: 11 September 2018

Please cite this article as: Jenine McCutcheon, Gordon Southam , Advanced biofilm staining techniques for TEM and SEM in geomicrobiology: Implications for visualizing EPS architecture, mineral nucleation, and microfossil generation. *Chemge* (2018), doi:[10.1016/j.chemgeo.2018.09.016](https://doi.org/10.1016/j.chemgeo.2018.09.016)

This is a PDF file of an unedited manuscript that has been accepted for publication. As a service to our customers we are providing this early version of the manuscript. The manuscript will undergo copyediting, typesetting, and review of the resulting proof before it is published in its final form. Please note that during the production process errors may be discovered which could affect the content, and all legal disclaimers that apply to the journal pertain.

Advanced biofilm staining techniques for TEM and SEM in geomicrobiology: Implications  
for visualizing EPS architecture, mineral nucleation, and microfossil generation

Jenine McCutcheon<sup>1,2\*</sup> and Gordon Southam<sup>1</sup>

<sup>1</sup>School of Earth and Environmental Sciences, The University of Queensland, St Lucia, QLD  
4072, Australia

<sup>2</sup>School of Earth and Environment, University of Leeds, Leeds, LS2 9JT, United Kingdom

\*Corresponding author: j.mccutcheon@leeds.ac.uk

A manuscript prepared for submission to: Chemical Geology

Keywords: biofilms; cyanobacteria; microbial mat; cryopreservation; TEM;  
biomineralization; electron diffraction; geomicrobiology; hydromagnesite; beachrock

### Highlights

- A multi-stain approach allows for biofilm EPS architecture to be observed using TEM
- SEM of thin sections hosting Os-stained biofilms reveals microbial microcolonies
- Hydromagnesite crystals nucleate on EPS tangential to cyanobacteria filaments
- Biofilm architecture visualization can aid mineral nucleation studies
- Modern biofilm mineralization processes can help elucidate microfossil generation

**Abstract**

Microbial biofilms and mats have long been studied for their role in mineral precipitation reactions in natural environments. Scanning electron microscopy (SEM) is often used to characterize biofilms and their associated precipitates, however, conventional SEM sample preparation methods do not typically preserve the structure of the extracellular polymeric substances (EPS), which account for a large portion of biofilm material and play critical roles in biofilm function and mineral nucleation. In the present investigation, three biofilm fixation and staining protocols were tested with regards to their ability to preserve, and aiding the visualization of, EPS using transmission electron microscopy (TEM). Although these protocols were initially developed for preserving complex tissue samples of eukaryotic organisms, the heterogeneous, three-dimensional nature of the biofilms make them suitable candidates for these sample processing methods. The results suggest that cryofixation provides the best preservation of cyanobacteria-dominated biofilm structures. A staining protocol including six different pre-embedding stains allowed for TEM visualization of the EPS matrix that encompasses biofilm cells and precipitate. Of the stains used, uranyl acetate appears to be critical in avoiding biofilm deformation during sample processing. Using these staining protocols, cell-EPS-mineral relationships were observed, including the precipitation of hydromagnesite  $[\text{Mg}_5(\text{CO}_3)_4(\text{OH})_2 \cdot 4\text{H}_2\text{O}]$  on the EPS adjacent to the cyanobacteria cell exterior. Beachrock-associated biofilms were characterized using both TEM of ultrathin sections, as well as SEM of resin embedded osmium stained biofilms prepared as petrographic thin sections. Combining these two approaches enabled characterization of both the micrometer-scale cell-carbonate mineral contacts, as well as the larger scale microbial colony-mineral cement relationships. These results suggest that sample preparation techniques developed for rapid preservation of eukaryotic tissue samples can be used to preserve and characterize biofilm architecture. These findings have applications to

understanding mineral nucleation in biofilms, and the preservation of biofilms as microfossils in the rock record.

## 1. Introduction

Geomicrobiology involves the study of microbe-mineral interactions, and the influence these interactions have on the geochemistry of natural environments (Ehrlich, 1998; Ehrlich, 1999). Due to the scale on which these biogeochemical relationships occur, microscopy and other microanalytical techniques have long been utilized in this field of study (Benzerara et al., 2006; Benzerara et al., 2014; Benzerara et al., 2004; Beveridge and Murray, 1976; Dupraz and Visscher, 2005; Dupraz et al., 2004; Fortin and Langley, 2005; Geesey et al., 2008; Kappler and Newman, 2004; Konhauser and Ferris, 1996; Li et al., 2016; Obst and Dittrich, 2005; Phoenix and Konhauser, 2008; Reid et al., 2000; Shuster et al., 2015; Southam, 2012; Southam and Beveridge, 1994). These techniques include confocal light microscopy, fluorescence microscopy, scanning (SEM) and transmission electron microscopy (TEM), atomic force microscopy, and various analyses using synchrotron radiation. Although recent advances of these techniques have enabled detailed characterization of structures and geochemical gradients generated at the interface of microbe-mineral relationships (Miot et al., 2014), the innate characteristic of geomicrobiological specimens to contain both biological and lithological components continues to present a challenge for sample preparation. Preserving these specimens can be especially difficult if the biominerals are redox sensitive, or require anoxic sample processing. The hydrated, fluid, and dynamic nature of the biofilms and microbial mats often targeted in geomicrobiology make them difficult to preserve. The challenge of maintaining the structure of extracellular polymeric substances (EPS) (Lawrence et al., 2003) and the microbe-mineral relationships that exist in hydrated biofilms has been the focus of several studies, which have primarily turned to cryogenic

techniques (Beveridge, 2006; Dohnalkova et al., 2011). These developments are based on the long known fact that cryo-preparation of biological samples results in better preservation of bacteria structures than chemical fixation (Graham and Beveridge, 1990a; Graham and Beveridge, 1990b; Graham et al., 1991; Miot et al., 2011). These techniques have recently been optimized such that they can be completed in a matter of hours (McDonald, 2007; McDonald, 2014). There has not, however, been any utilization of these faster processing protocols in the field of geomicrobiology, leaving the field of TEM examination of natural microbial biofilms underdeveloped.

The complex challenge of characterizing biofilm samples is compounded by the fact that even if the biofilm is accurately preserved, the chemistry and mineralogy of the nano- to micrometer sized mineral crystals often precipitated in biofilms is difficult to analyze. Adsorption of metals to bacterial cell envelopes (Beveridge and Murray, 1976), the ability of cells and EPS to act as nucleation sites for mineral precipitation (Braissant et al., 2007; Dupraz et al., 2009; Gallagher et al., 2012; Shuster et al., 2015; Southam and Beveridge, 1994), and the formation of intracellular mineral precipitates (Benzerara et al., 2014; Cam et al., 2016; Cam et al., 2018; Komeili et al., 2004) make it critical to maintain both biofilm structure, mineral precipitate structure and redox state, such that the whole specimen can be imaged and analyzed in a single sample. Only by achieving this can microbe-mineral interactions be thoroughly characterized.

In the presented study, a variety of preservation techniques were applied to cyanobacteria-dominated biofilms for characterization using TEM, as well as explore the use of electron diffraction as a means of identifying hydrated magnesium carbonate minerals in these biofilms. Three protocols were used to examine preservation and staining of cyanobacteria biofilms, thereby we first examine the difference in biofilm preservation using cryo- versus chemical-fixation, and second compare the staining of extracellular structures in

the biofilm, with the goal of optimizing the quality of both preservation and staining. Additionally, samples of beachrock-hosted biofilms provided an example how the third staining protocol can be applied to a mineral-bearing complex natural biofilm.

## 2. Methods

**2.1 Scanning electron microscopy of non-mineralized biofilms.** A cyanobacteria biofilm was grown in the laboratory in BG-11 growth medium (Vonshak, 1986), sourced from a microbial mat sample collected from pit waters in the Woodsreef Asbestos Mine, NSW, Australia (McCutcheon et al., 2017b; McCutcheon et al., 2016b). The biofilm was fixed using 2.5% glutaraldehyde prior to an ethanol dehydration (20%, 40%, 60%, 80%, 100%, 100%, 100%) using a Pelco Biowave (Tedpella, Redding, CA) microwave (no vacuum, 250 W, 40 s each step), followed by critical point drying using a Tousimis Samdri-PVT-3B critical point dryer (Tousimis, Rockville, MD). The samples were mounted on stainless steel SEM stubs using adhesive carbon tabs and coated with 4 nm of osmium using a Filgen OPC80T osmium plasma coater (Filgen, Inc., JP). The samples were observed and imaged using secondary-electron SEM (SE-SEM) using a Zeiss Leo 1540 XB (Carl Zeiss, Jena, DE).

**2.2 Biofilm preservation and staining techniques for TEM.** The three protocols used to preserve and stain the cyanobacteria Woodsreef Mine biofilm sample, hereafter referred to as Protocols 1, 2 and 3, are outlined in Figure 1.

### 2.2.1 Protocol 1.

Fixation: the biofilm sample was fixed by high-pressure freezing (HPF) using a Leica EM Pact2 high-pressure freezer (Leica Biosystems, Wetzlar, DE). The samples were added to 0.7% (wt./vol.) Type VII agarose in 100  $\mu$ m deep Au-coated Cu specimen carriers prior to being high-pressure frozen using the protocol described by McDonald and Webb (2011).

Staining: the HPF step was followed by the quick freeze substitution method outlined by McDonald and Webb (2011), using a solution of 1%<sub>(aq)</sub> osmium tetroxide (OsO<sub>4</sub>), 0.5%<sub>(aq)</sub>

uranyl acetate (UA), and 5% (vol./vol.) water in acetone, contained in a liquid nitrogen-filled Styrofoam™ container set on a platform shaker operated at 125 rpm (McDonald, 1999).

Solvent: following staining, the samples were washed in 100% acetone.

Resin-infiltration: the samples were embedded in Epon EMBED 812 Resin (Luft, 1961) (Electron Microscopy Sciences (EMS), Hatfield, PA) using Epon:acetone mixtures of 20, 40, 60, 80, 90, 100, 100, 100 in the Biowave microwave at 250 W with the vacuum on, with the microwave on for 2 min, then off for 2 min, then on for 2 min for each step, after which the Epon was cured at 60°C for 48 h. Note, the microwave steps are longer in duration than typically used for embedding to ensure complete infiltration of resin into the cells.

Ultrathin sectioning: the resin blocks were trimmed, and cut into 70 nm thick ultrathin sections using an Ultra 45° DiATOME diamond knife (DiATOME, Hatfield, PA) and a Leica Ultracut UC6 ultramicrotome (Leica Biosystems, Wetzlar, DE), and collected on 200 mesh Formvar-carbon coated copper grids.

Post-stain: none.

#### 2.2.2 Protocol 2.

Fixation and staining: the biofilm sample was fixed using 2.5% glutaraldehyde and 2.0% paraformaldehyde while concurrently being stained with 75 mM L-lysine and 0.075%<sub>(aq)</sub> ruthenium red in a 0.1M sodium cacodylate buffer (Figure 1) (Fassel et al., 1998). The lysine solution was made using L-lysine monohydrochloride. Both solutions were made using a cacodylate buffer after which they were mixed together and the sample was immediately placed in the combined solution. The sample was left in the fixative for 2 h at 4°C, after which it was rinsed with 0.1 M sodium cacodylate buffer.

Additional staining: after the 2 h fixation, the biofilm was rinsed with 0.1 M sodium cacodylate buffer and stained using 2.0%<sub>(aq)</sub> OsO<sub>4</sub> using the Biowave (vacuum on, 80 W, 2 × [2 min on, 2 min off, 2 min on]) (Garland et al., 1975).

Solvent: the sample was dehydrated using an ethanol dehydration series at concentrations of 20%, 40%, 60%, 80%, 90%,  $3 \times 100\%$  using the Biowave (no vacuum, 250 W, 40 s each step).

Resin-infiltration: The sample was then embedded as described in Protocol One, with the exception that the Epon-solvent mixtures contained ethanol rather than acetone.

Ultrathin sectioning: as outlined in Protocol 1.

Post-stain: following ultrathin sectioning, the grids were post-stained using Reynolds' lead citrate (Reynolds, 1963).

### 2.2.3 Protocol 3.

Fixation and staining: as outlined in Protocol 2.

Additional staining: the biofilm sample was rinsed with phosphate buffered saline (PBS) (Biowave: vacuum on, 80 W,  $2 \times 40$  s) and further stained with osmium, ferricyanide and thiocarbohydrazide, a modified version of the protocol described by Holcomb et al. (2013); a staining procedure developed for 3D reconstruction of brain tissue. This multi-stain approach combines stains for which there have been individual protocols for a number of years (McDonald, 1984; Palade, 1952; Seligman et al., 1966; Watson, 1958). To the best of our knowledge, however, there has been little use of this particular combination of stains in geomicrobiology. Briefly, the sample was sequentially stained using:  $2\%_{(aq)}$   $\text{OsO}_4$  and  $1.5\%_{(aq)}$  ferricyanide (Biowave: vacuum on, 80 W,  $2 \times [2 \text{ min on, } 2 \text{ min off, } 2 \text{ min on}]$ ); rinsed with UHQ water (once on the bench, once in the Biowave: vacuum on, 80 W,  $2 \times 40$  s);  $1\%_{(aq)}$  thiocarbohydrazide (TCH) (Note, TCH takes 1 h to dissolve at  $60^\circ\text{C}$  with agitation every 10 min; once dissolved, the sample was stained for 20 min); rinsed with UHQ water (once on the bench, once in the Biowave: vacuum on, 80 W,  $2 \times 40$  s). Due to the toxicity of TCH, the sample was placed in a new sample tube to minimize additional TCH contamination of the sample processing materials. Samples were then stained with  $2\%_{(aq)}$

OsO<sub>4</sub> using the Biowave (vacuum on, 80 W, 2 × [min on, 2 min off, 2 min on]); rinsed with UHQ water (once on the bench, once in the Biowave: vacuum on, 80 W, 2 × 40 s); 1%<sub>(aq)</sub> uranyl acetate (Watson, 1958) (vacuum on, 150 W, 2 × 2 min on, 2 min off, 2 min on); and rinsed with UHQ water (once on the bench, once in the Biowave: vacuum on, 80 W, 2 × 40 s).

Solvent: as outlined in Protocol 2.

Resin-infiltration: as outlined in Protocol 1.

Ultrathin sectioning: as outlined in Protocol 1.

Post-stain: none.

**2.3 Transmission electron microscopy.** All samples were characterized using a JEOL-JEM 1011 TEM (JEOL Ltd., Akishima, JP) equipped with an Olympus Soft Imaging Solutions Morada CCD camera at 80 kV, and a JEOL-JEM 1010 TEM equipped with an Olympus Soft Imaging Solutions Veleta 2K × 2K wide angle digital camera at 80 kV.

**2.4 Characterization of cyanobacteria-hosted hydromagnesite using TEM-SAED.** A second cyanobacteria-dominated biofilm sample from a natural consortium known to precipitate hydromagnesite [Mg<sub>5</sub>(CO<sub>3</sub>)<sub>4</sub>(OH)<sub>2</sub>·4H<sub>2</sub>O] (McCutcheon et al., 2014) was fixed using 2.5% glutaraldehyde and stained using a modified version of Protocol 3. As the sample was already fixed prior to staining, the lysine-ruthenium red step was excluded because this step typically occurs concurrently with aldehyde fixation. Additionally, the uranyl acetate steps was omitted because these stains are too acidic for use on samples containing carbonate. In some cases, in which pH is a concern, osmium tetroxide should also be omitted. These changes need not be made for biofilms containing minerals stable at low pH values. Sample dehydration using ethanol and resin infiltration using Epon was continued as described in Protocol 3. Selected area electron diffraction (SAED) was conducted using a JEOL-JEM 2100 TEM at 120 kV equipped with a Gatan Orius 1000 slow scan CCD camera (Gatan Inc.,

Pleasanton, CA). The lattice spacing measured from the SAED patterns were compared to known lattice data for hydromagnesite (ICDD, 1975).

**2.5 Characterization of beachrock biofilms and calcium carbonate precipitates.** Microbial mats and biofilms found on, and within, the beachrock on Heron Island (Capricorn Group, Great Barrier Reef, Australia) have been previously studied for their ability to precipitate calcium carbonate cements and form microbialites (McCutcheon et al., 2016a; McCutcheon et al., 2017a; Webb et al., 1999). A sample of the cyanobacteria-dominated microbial mat hosting abundant carbonate mineral grains was collected from the surface of the beachrock and prepared using the protocol outlined in Section 2.1. A second surface beachrock-biofilm sample was stained using 2%<sub>(aq)</sub> OsO<sub>4</sub> prior to being processed through an ethanol dehydration series at concentrations of 20%, 40%, 60%, 80%, 90%, 100%, 100%, 100% using the Biowave (no vacuum, 250 W, 40 s each step). Once dehydrated, the sample was embedded in Epon EMbed 812 Resin, and prepared as polished petrographic thin sections. Thin sections were characterized using back-scattered electron (BSE) SEM, in conjunction with energy dispersive spectroscopy (EDS) using an Oxford Instruments (Abingdon, UK) INCA x-sight energy dispersive spectrometer. A third sample of beachrock biofilm was processed using the modified version Protocol 3 described in Section 2.4, in which the lysine-ruthenium red and uranyl acetate steps were excluded, prior to observation using TEM.

### 3. Results

**3.1 Scanning electron microscopy of non-mineralized biofilms.** SEM of the Woodsreef Mine biofilm sample confirmed that it primarily contained filamentous cyanobacteria, with associated heterotrophs (Fig. 2A,B). Large quantities of EPS can be seen (Fig. 2C), which is visible as mesh-like fibers on cell surfaces. Although the EPS is retained through sample

preparation, its structural integrity was compromised during the dehydration, and its structure as a hydrated gel is not preserved.

**3.2 Biofilm fixation and staining protocol comparison using TEM.** The three protocols by which the Woodsreef biofilm samples were processed resulted in varying degrees of preservation and structure visualization when observed using TEM. The HPF-freeze substitution protocol (protocol one) provided the best preservation of cyanobacteria cell structures, particularly thylakoids and carboxysomes, although little can be seen of EPS or other extracellular features (Fig. 3A,B). In contrast, Protocols 2 and 3 provided better staining of the extracellular features of the biofilm. Protocol 2 provided good contrast of thylakoids, carboxysomes, and exopolymer (Fig. 3C,D). It appears, however, that this protocol resulted in some deformation of the EPS structure, with the EPS beginning to develop the fiber-like morphology often seen as an artefact of specimen preparation for SEM (Fig. 2C). Protocol 3 provided the best contrast of the biofilm, and appears to have maintained the gel-like structure representative of EPS in live cultures (Fig. 3E,F). The third protocol is also preferable over the second with regards to staining of cyanobacteria cell structures such as the cell envelope, thylakoids, and carboxysomes (Fig. 3,4). In Figure 3E,F, note the clear visualization of the thylakoids, carboxysomes, and what appear to be polyhydroxybutyrate (PHB) granules. The staining of the thylakoids and other cell structures by Protocol 2 resulted in a grainy appearance (Fig. 4A,B), an artefact not observed for those stained using Protocol 3 (Fig. 4C,D).

### **3.3 Characterization of mineral precipitates in biofilms.**

**3.3.1 Cyanobacteria and hydromagnesite.** The precipitates observed in the biofilm sample appeared to primarily form on the EPS that encapsulates cyanobacteria cells, precipitating such that the crystals are oriented tangential to filament surfaces (Fig. 5A-D). This is consistent with the typical presentation of this filament-mineral association as seen using

SEM (Fig. 5E,F). SAED of the precipitates in this orientation was difficult, as only the edges of the ~20 nm thick platy crystals were accessible for diffraction, providing a very limited detectable sample volume within the confines of the 70 nm-thick section. SAED generated a limited set of diffraction spots (Fig. 5D, inset), the lattice spacings of which were consistent with known values for hydromagnesite (Table 1). While it is not ideal diffraction data, this is, to our knowledge, the first in situ identification of biologically mediated hydromagnesite precipitates using electron diffraction.

3.3.2 Beachrock biofilm and calcium carbonate. SE-SEM of the beachrock biofilm revealed a heterogeneous assortment of intermixed cells, EPS, and mineral grains (Fig. 6A). When observed as a polished thin section using BSE-SEM, it becomes apparent the microbial cells, including filamentous cyanobacteria, are systematically organized in microcolonies (Fig. 6B). A sample of fractured beachrock viewed using SE-SEM reveals the presence of microfossils of filamentous cyanobacteria, visible as mineralized molds of the microbial cells (Fig. 6C,D). Using SEM, nothing can be discerned of the pre-mineralization biofilm structure. In contrast, TEM of a non-mineralized portion of the beachrock biofilm reveals the complex heterogeneous nature of the sample, containing larger filamentous cyanobacteria, smaller heterotrophs, remnants of lysed cells, and EPS (Fig. 6E,F).

BSE-SEM of the polished thin section of beachrock biofilm revealed abundant filamentous cyanobacteria, which in some cases, contain micrometer to sub-micrometer-scale intracellular bodies (Fig. 7A,B) stained with osmium, and interpreted as PHB granules. Much smaller granules were also observed colocalized with the thylakoid membranes of a lysed cell using TEM (Fig. 7C,D,E). The remains of the cell envelope and EPS can also be observed in Figure 6F, on which extracellular carbonate precipitates, such as those in Figure 8, tend to form. Micritic extracellular calcium carbonate precipitates can be observed using BSE-SEM among the densely packed microcolonies (Fig. 8A). Similar to the hydromagnesite in Figure

5, these precipitates are located on the EPS that can be seen surrounding the cells (Fig. 8B). These precipitates are composed of Ca-Mg-C-O, as indicated by the representative EDS spectrum overlain on Figure 8B. The cell-EPS-mineral grain relationship is better viewed using TEM (Fig. 8C,D). The cell is encapsulated in a mineral-free envelope of EPS, outside of which the precipitates can be seen (Fig. 8D).

#### 4. Discussion

**4.1 Biofilm visualization: intracellular versus extracellular structures.** SEM of the biofilm shows the collapse of EPS often documented when biofilm samples are processed using a solvent dehydration series and subsequent critical point drying, thus demonstrating one of the reasons for pursuing this investigation (Fig. 2) (Dohnalkova et al., 2011). Examining the structure of a biofilm using TEM requires preservation using either chemical or cryogenic methods. Although cryogenic methods of sample fixation are known to better preserve cell structures (Graham and Beveridge, 1990a; Graham and Beveridge, 1990b; Graham et al., 1991; McDonald, 1999; McDonald, 2014; Miot et al., 2011), chemical fixation is more common in geomicrobiology, likely because it is more practical for immediately preserving samples collected from the natural environment. Sample collection from remote field locations may necessitate the use of chemical fixation; however, cryogenic methods would be preferable for use in laboratory studies as they provide instantaneous, and more accurate, preservation of cellular structures (McDonald, 2014). Previous studies applying cryofixation and freeze-substitution to cyanobacteria samples have primarily focused on internal cell structure rather than extracellular features, particularly EPS, occurring in biofilms (Hoiczky and Baumeister, 1995; Mehta et al., 2015). The present study has demonstrated that high-pressure freezing achieves good quality visualization of cell ultrastructures, such as the

carboxysomes shown in Figure 3A, but that metal fixatives, such as ruthenium red, are required to visualize EPS.

Interestingly, as many as 20 carboxysomes can be observed per cyanobacterial cell, which is on par with the maximum number of carboxysomes observed in cyanobacteria (Li et al., 2016). These carboxysomes are up to 500 nm in diameter, which is consistent with the  $\beta$ -carboxysomes typically observed in freshwater cyanobacteria (Rae et al., 2013). The abundance of carboxysomes in the cyanobacteria in this culture is of interest, as this culture was sourced from a microbial biofilm growing in a chrysotile mine pit lake that was collected for the purposes of studying microbial carbonation reactions (McCutcheon et al., 2016b). Carboxysomes house the enzyme ribulose-1,5-bisphosphate carboxylase/oxygenase (RuBisCO), which is critical to the CO<sub>2</sub>-concentrating mechanism (CCM) utilized by cyanobacteria to encourage the carboxylase step at the beginning of the Calvin Cycle (Rae et al., 2013). In the context of microbial carbonation, the proteinaceous shell of carboxysomes have been suggested to act as a nucleation site for intracellular carbonate precipitation (Li et al., 2016), and consequently, it is worth refining the cryogenic methods capable of better visualizing these intracellular structures.

Other intracellular features can be observed using TEM, including what appear to be PHB granules in Figure 3E,F, similar to those documented by Zhang et al. (2014) and Damrow et al. (2016). Although the sample was sourced from a different environment than the sample depicted in Figure 3, some of the osmium-stained, 'electron dense' bodies observed in the Heron Island beachrock biofilm using BSE-SEM may also be PHB granules (Fig. 7A,B). These hydrophobic storage molecules are typically 200-500 nm in size (Reusch, 2012), can account for up to ~6% dry weight of cells (Ansari and Fatma, 2016), and are known to bind calcium, as indicated by EDS analysis in the present study (Fig. 7B, overlain) (Reusch and Sadoff, 1988). The formation of PHB is often triggered by macronutrient

limitation stress, such as a lack of nitrogen or phosphorous (Damrow et al., 2016; Madison and Huisman, 1999). The smaller, electron-dense granules observed colocalized with the remnants of the thylakoid membranes using TEM (Figure 7C-E), may be glycogen granules similar to those observed by Yamauchi et al. (2011) and Yu et al. (2015). These carbon biopolymers are water-soluble and are typically an order of magnitude smaller than PHB granules (Damrow et al., 2016), though similarly, they are also generated during nutrient-limiting growth conditions (Damrow et al., 2016; Yamauchi et al., 2011). Interestingly, PHB is less commonly used by cyanobacteria as a storage molecule compared to glycogen, and microbes typically only produce one or the other type of granule (Beck et al., 2012). Consequently, while both types of granules indicate the same environmental stressor, the PHB and glycogen bearing filaments likely represent different cyanobacterium species in the Heron Island beachrock biofilm community (McCutcheon et al., 2016a).

In comparison to cryogenic methods, chemical fixation still provides adequate preservation of the biofilm and cellular structures, and is more suitable as a method to precede the staining techniques used in Protocols 2 and 3. The ‘grainy’ texture observed in the biofilm prepared using Protocol 2 is likely due to the lack of a UA step in this protocol. A UA step is typically included in conventional sample preparation protocols, and appears to be important in achieving complete fixation of cellular materials such that condensation, and production of these granular features within the cytoplasm, does not occur. This finding is consistent with that presented by McDonald (1984), in which UA was found to stabilize delicate cell structures throughout the dehydration and embedding steps. Protocol 3 provided the best staining of the extracellular aspect of the biofilm, when compared to the more traditional stains used in Protocol 1 and 2. Combining the high-quality preservation of intracellular structures achieved using cryofixation, with the detailed contrast of EPS and extracellular features attained using the stains in Protocol 3 for EPS would likely provide the

best result for visualizing overall extracellular biofilm structures. Such a method, however, has not yet been developed.

**4.2 Biofilm dehydration and resin infiltration.** One of the main challenges of preserving biofilms is the hydrated nature of EPS. EPS is adept at retaining water, making it difficult to thoroughly dehydrate. Attempting to embed an incompletely dehydrated biofilm in most resins will result in poor polymerization of the resin. This problem is partially abated by using the microwave for infiltration of the sample by stains, solvents, and resins alike, rather than relying on ambient diffusion (Boon et al., 1986). Use of a microwave is especially beneficial when it is combined with a vacuum, particularly for resin infiltration (McDonald and Webb, 2011). If infiltration problems persist, increasing the number steps in the ethanol dehydration series and resin infiltration can reduce the effects. Increasing the number of steps taken to dehydrate the sample with the solvent; however, can result in increased disruption of structures in the sample (Graham and Beveridge, 1990b). As a result, it is preferable to use the fewest possible steps to achieve complete dehydration and infiltration of the sample, which may need to be determined on a per sample basis. As mentioned in the methods, the duration of the resin infiltration steps in the present study were increased, a decision made based on poor infiltration results previously achieved when a shorter microwave steps was used (results not shown).

**4.3 Biofilms as three-dimensional structures.** TEM of traditional microbiological samples often focus on monocultures grown in the laboratory, typically with the goal of characterizing individual cellular structures (Beveridge and Graham, 1991; Graham and Beveridge, 1990a; Hoiczky and Baumeister, 1995; Southam et al., 1993). These methods have been adapted for use in geomicrobiology, most simply by removing the use of metals in fixation or staining. Such modifications are necessary when processing redox sensitive samples, as some stains, such as osmium tetroxide, are strong oxidizing agents. Although these methods are useful,

they do not account for the extracellular features of complex, heterogeneous microbial biofilms (Fig. 6E,F), or the relationship between these biofilms and any mineral precipitates they may contain (Fig. 7,8). In spite of the fact that the EPS matrix accounts for up to 90% of the total organic carbon of biofilms (Frølund et al., 1996), it is often overlooked in TEM sample preservation techniques. EPS is composed of water, polysaccharides, proteins, lipids, and nucleic acids (Flemming and Wingender, 2010). This material plays a critical role in biofilm function, aiding with: biofilm stability and adhesion to surfaces, cell aggregation enabling cell-cell interaction and lateral gene transfer, water retention, sorption of organic molecules and inorganic ions, and providing a source and sink for excess energy and nutrients (Flemming and Wingender, 2010). The structural integrity of EPS is largely provided by polysaccharides, allowing it to support the cells from which it is derived. Cross-linking of the polysaccharides with ions in solution, such as alginate with  $\text{Ca}^{2+}$ , can cause an increase in the mechanical stability of the biofilm (Körstgens et al., 2001). Such interactions are useful in natural biofilms as these ions become available for the precipitation of minerals (Braissant et al., 2007; Braissant et al., 2009), such as the calcium carbonate precipitation observed in Figures 7 and 8. The structural integrity also changes in response to environmental stressors, such as temperature, desiccation, UV radiation, and shear stress (Flemming and Wingender, 2010). Desiccation instigates the production of EPS, and concurrently reduces the volume of the biofilm, causing cross-linking of non-specific binding sites (Potts, 1994; Roberson and Firestone, 1992). The tendency for desiccation to induce EPS produce may, in part, explain the copious amounts of EPS observed in the Heron Island biofilms (Fig. 6-8), as these biofilms were sampled from an intertidal habitat that would have been subjected to tide-induced wetting and drying cycles. Extracellular enzymatic activity is important for degradation of organic compounds to low-molecular weight products that can be utilized by the cells in the biofilm as sources of carbon and energy (Flemming and

Wingender, 2010). In nutrient limited conditions, degradation of the EPS itself can act as a nutrient source for the biofilm inhabitants while concurrently altering the matrix structure (Braissant et al., 2009; Decho et al., 2005). The presence of the PHB and glycogen granules in the Heron Island biofilms indicate that nutrient limiting growth conditions may have presided, in which case EPS may also have acted as an emergency energy store for the microbes in these biofilms.

Additionally, natural microbial mats typically contain numerous different types of microorganisms, both prokaryotes and eukaryotes, all at various stages of their life cycle (Visscher and Stolz, 2005), as demonstrated in Figure 6E,F. Organisms are often situated within microbial mats based on metabolism, such that: oxygenic phototrophs are near the surface, methanogens or acetogens are at the bottom, and a range of intermediate metabolic strategies interspersed along the geochemical gradient found between these end members (Jørgensen and Des Marais, 1986; Jørgensen et al., 1979; Visscher and Stolz, 2005). A result of this metabolic stratification is a corresponding change in pore fluid chemistry (de Beer et al., 1994; Glud et al., 1992; Stewart and Franklin, 2008).

The product of these spatial heterogeneities of cell type, metabolism, fluid geochemistry, and extracellular matrix is a truly three-dimensional structure. In this sense, microbial mats are more akin to the complex tissue samples of eukaryotic organisms than the bacteria monocultures with which they are often lumped due to both being composed of 'microbes'. Three-dimensional reconstruction of tissue samples of eukaryotic organisms is common practice, with extensive methods development recently taking place in the fields of plant and animal tissue reconstruction (Gillies et al., 2014; Haley and Lawrence, 2016; Kittelmann et al., 2016; Mouw et al., 2014; Randles et al., 2016; Starborg and Kadler, 2015; Starborg et al., 2013; Young et al., 2014). These advances in technique development, however, have seen little use in geomicrobiology. This may, in part, be the product of a

division between research fields known for TEM sample preparation expertise, such as neurobiology, and the fields of research interested in natural biofilm samples that are found largely within the geosciences. As a result, although biofilms and microbial mats are the focus of numerous biogeochemical studies, these materials are often processed using techniques more appropriate for rock, soil, or sediment samples. This dichotomy between research fields and sample preparation protocols means that technique development for examining natural biofilms using TEM has remained underdeveloped. Only by visualizing all of the extracellular components can the architecture of the biofilm be constrained.

**4.4 Mineral precipitation in biofilms.** Once EPS can be seen, it becomes possible to observe where minerals are forming within a biofilm, observations that are critical to understanding mineral nucleation processes. In this investigation, the hydromagnesite crystals appear to be precipitating directly on the EPS encapsulating the cyanobacterial cells (Fig. 5A-D). It appears that, in some cases, the EPS and attached crystals are then shed from the cell exterior (Fig. 5C,D). Capturing the orientation of these crystals gives us an indication of where they nucleated with respect to the cyanobacterial filament. This orientation, however, made it difficult to identify the phase using SAED, as only the hydromagnesite crystal cross-section can be seen and analyzed, rather than the crystal face.

The presence of mineral precipitates may, in part, be the reason why new staining methods have not been applied in the field of geomicrobiology. In some cases, natural biomineralization is considered a means of ‘staining’ cells and seemingly eliminates the need for further staining. This is useful for some precipitates, such as iron oxides, which adequately highlight cell exteriors (Fortin and Langley, 2005; Langley et al., 2009). In samples in which mineralization is not pervasive, it is a possible that extracellular structures not coated in mineral precipitates are being overlooked. This is particularly true in nucleation studies; biofilms that are completely mineralized cannot provide information on where in the

biofilm nucleation starts. In this case, it is desirable to have minimal precipitation, along with which a geochemically compatible stain must be applied to highlight the biofilm architecture that is not yet mineralized. In the case of carbonate minerals, pH sensitivity eliminates the use of several traditional staining methods. Lead aspartate and uranyl acetate are acidic, making mineral dissolution a risk, while Reynolds' lead citrate has a high pH and will precipitate on the ultrathin section in carbonate-bearing samples. A comprehensive investigation matching staining protocols to particular geochemical systems and corresponding mineral products would be a valuable contribution to the current literature.

Visualizing the onset of mineral nucleation in biofilms is crucial to understanding fossilization, as such samples are the forerunners to the mineralized biofilms preserved in the rock record over geologic time scales. In the context of fossilization, as the mineralized skeletons of eukaryotic organisms are more readily preserved than soft body tissue, mineralized biofilms in the form of micro- or macro-fossils, represent a microbiological 'hard body tissue', that is much more likely to be preserved than their non-mineralized counterparts. Observing contemporary biofilms in the early stages of mineralization can aid in understanding the biogeochemical controls on biofilm cementation processes that result in structures such as microbialites and stromatolites (Burne and Moore, 1987; Pace et al., 2018; Riding, 2000). Petrographic thin sections made from embedded sections osmium-stained samples of rock-associated biofilm provide a good means of observing these biofilm-rock contacts on a larger scale than what can be achieved using TEM, as demonstrated in Fig. 5B, 6A,B, and 7A,B.

The beachrock sample depicted in Figures 6-8 provide a contemporary example of the progression from a complex natural biofilm, through calcium carbonate mineral nucleation and precipitation, to a fossilized biofilm such as what may be preserved in the rock record. The heterogeneous biofilm consists of filamentous cyanobacteria, colonies of heterotrophs,

lysed cells, and abundant EPS, all of which are intermixed with mineral grains (Fig. 6E,F). Mineral nucleation can be observed in the beachrock biofilm samples as extracellular precipitates (Fig. 6) that appear to have formed on the EPS surrounding the cells (Fig. 8C,D). Notably, there is an expanse of EPS void of any minerals immediately surrounding the cell, outside of which the mineral grains can be seen. This cell-EPS-mineral relationship is comparable to that observed for the hydromagnesite precipitating biofilm described above, and may be the product of these organisms generating EPS as a mechanism to ‘shed’ their extracellular precipitates, thus avoiding becoming encased in carbonate cement.

It is worth noting that some of the mineral grains here observed may not be new precipitates that have nucleated within the biofilm, rather, detrital grains that have been trapped and bound by the biofilm EPS. Adhesion of sediment grains to biofilms through trapping and binding has been observed in stromatolites representing some of the earliest evidence of microbial life in the rock record (Altermann, 2008). This mechanism, combined with cement precipitation, can encase cells such that cemented molds of the filaments remain as microscopic ichnofossils of the biofilm (Fig. 6C,D). Once, mineralization has occurred, the complexity of the three-dimensional biofilm architecture is lost, thus demonstrating the need for further visualization of the mineralizing features, including EPS and lysed cells, in complex biofilm samples using TEM.

## 5. Conclusions

Three different protocols were used to prepare microbial biofilm samples in order to determine the ability of each protocol to aid in the visualization of extracellular biofilm features, particularly EPS. Cryofixation provided the best preservation of cellular structures (Protocol 1), while chemical fixation plus as many as six subsequent staining steps (Protocol 3) provided the best overall visualization of EPS. It appears that uranyl acetate is important

for preserving cell structure throughout sample dehydration and embedding, as the biofilm samples prepared without UA exhibited condensation defects.

The preservation and staining methods explored in this study provide better visualization of both intracellular and extracellular features of biofilms, particularly EPS, than conventional protocols often used for biofilm preparation. Achieving better visualization of EPS is crucial because EPS is the focus of many biomineralization investigations. Visualization of EPS within a biofilm allows for a better understanding of the three-dimensional architecture that surrounds and supports individual cells. In the present study, biofilms stained with osmium, embedded in resin, and made into petrographic thin sections provide a valuable means of observing and characterizing larger sections of biofilm or microbial mat, thus enabling the visualization of cyanobacteria microcolonies, as well as the presence of intercellular micritic cements precipitated on EPS. Determining the location of mineral nucleation within a microbial mat can provide insight into the intricate interactions taking place between the microbial cells, their extracellular structures, the surrounding water chemistry, and the resultant mineral precipitates. In the present study, the precipitation of hydromagnesite crystals on EPS, oriented tangential to filamentous cyanobacteria cells, was observed.

Although microbial biofilms and mats have been acknowledged as complex structures, the conventional microbiology TEM sample preparation methods being used to study these samples have focused on highlighting internal cellular features and do not always make it possible to visualize the complex extracellular features. In order to change this, it is necessary to treat these materials as complex, spatially heterogeneous three-dimensional structures not unlike tissue samples of eukaryotic organisms.

## Acknowledgements

Sample preparation and TEM was conducted at the Centre for Microscopy and Microanalysis (CMM, The University of Queensland). We thank Kathryn Green, Richard Webb, Robyn Webb, and Graeme Auchterlonie of CMM for their technical assistance. SEM was conducted at the Nanofabrication Facility (The University of Western Ontario). We thank Sasha Wilson and Jeremiah Shuster for helpful discussions about electron diffraction and TEM. J. McCutcheon was supported by a National Sciences and Engineering Research Council of Canada PhD Postgraduate Scholarship. Funding to G. Southam was provided in part by Carbon Management Canada.

## Figure Captions

Figure 1. Summary of the key steps in the three protocols used to fix and stain cyanobacteria biofilms for TEM. Summary of useful references for various aspects of these protocols.

Figure 2. Secondary electron scanning electron micrographs displaying A) the biofilm used in the stain comparison investigation. The biofilm is composed of B) filamentous cyanobacteria cells and associated coccoid heterotrophs found coated with EPS. C) EPS appears as a collapsed mesh on the surface of the cells, representing a classic morphology that is actually an artefact of the sample preparation process.

Figure 3. Transmission electron micrographs showing the results of preparing the cyanobacteria biofilm using A,B) protocol one: high-pressure freezing, freeze substitution, osmium tetroxide, and uranyl acetate; C,D) Protocol 2: glutaraldehyde, paraformaldehyde, lysine, ruthenium red, osmium tetroxide, and a lead post-stain; and E,F) protocol three: glutaraldehyde, paraformaldehyde, lysine, ruthenium red, osmium tetroxide,

thiocarbohydrazide, lead aspartate, osmium tetroxide, and uranyl acetate. High-pressure freezing provided the best preservation (protocol one), while the staining in protocol three provided the best visibility of extracellular features of the biofilm. In A) note the abundant carboxysomes per cell (arrow). In B,D,F) C: carboxysomes, T: thylakoid, PHB: polyhydroxybutyrate granule.

Figure 4. Transmission electron micrographs showing the staining of the cyanobacteria cells using A,B) Protocol 2: glutaraldehyde, paraformaldehyde, lysine, ruthenium red, osmium tetroxide, and a lead post-stain; C,D) protocol three: glutaraldehyde, paraformaldehyde, lysine, ruthenium red, osmium tetroxide, thiocarbohydrazide, lead aspartate, osmium tetroxide, and uranyl acetate. Protocol 2 left the sample with a grainy texture consistent with the precipitation of lead, while protocol three produced uniformly stained cells.

Figure 5. Transmission electron micrographs revealed the precipitation of hydromagnesite on EPS adjacent to cyanobacteria filaments (A,B). Note, the precipitates, which are primarily oriented perpendicular to the plane of the ultrathin section (C,D), with the mineral plane aligned with the filament surface, such that only the edge of the crystals can be seen, and in some cases, these minerals appear to be detaching, being shed from the cell envelope. This orientation makes them difficult to target with SAED (inlay of D, circles indicate visible diffraction spots, numbers relate to lattice spacings listed in Table 1). E) SE-SEM of the sample shows the same cyanobacteria-EPS-hydromagnesite relationship for small hydromagnesite platelets; however, the structure of the EPS is lost due to dehydration of the sample. F) SE-SEM of platy hydromagnesite crystals oriented tangential to a filamentous cyanobacterium; a similar spatial relationship as observed using TEM in A-D.

Figure 6. Scanning electron micrographs of the outer surface of the Heron Island beachrock biofilm (see McCutcheon et al. (2016a)) revealing the complexity of a natural biofilm (A). When viewed as a polished thin section (B), it can be observed that the biofilm is organized in microcolonies. Secondary electron SEM of a mineralized section of biofilm that has broken open, reveals microfossils in the form of mineralized molds of the filamentous cyanobacteria in carbonate cement (C,D). Note, the inside of the biofilm cannot be easily seen using secondary electron imaging. Transmission electron micrographs (E,F) illustrating the heterogeneity of the cyanobacteria-dominated biofilm including the presence of empty cell envelopes (arrows), which cannot be seen using BSE imaging, and the much smaller heterotrophs (circled) among the EPS matrix.

Figure 7. Scanning electron micrographs (A,B) of a polished thin section of embedded microbial biofilm growing on the Heron Island beachrock revealing filamentous cyanobacteria containing intracellular bodies interpreted as polyhydroxybutyrate (PHB), visible as electron dense granules (bright white in BSE-SEM). EDS analysis (overlain on B) of the granule in the filament indicated with an arrow (B). Note, the S and Cl peaks identified using EDS are a product of the resin, and the Os is a product of the stain used during sample preparation, which targets hydrophobic materials. Smaller, electron-dense (black) intracellular granules observed using TEM (C,D). These granules (arrows) appear to be adhered to the remnants of the thylakoids (E). Transmission electron micrograph (F) illustrating the complex structure of the EPS on which extracellular mineral precipitates form (Figure 7).

Figure 8. Back-scattered electron micrographs of a polished thin section of embedded Heron Island beachrock biofilm revealing microcolonies of cells around which extracellular micritic

mineral grains can be observed (bright white in BSE-SEM) (A). These grains can be observed forming on the exterior of the EPS encapsulating cells (B). A representative EDS spectrum indicating the Ca-Mg-C-O composition of these precipitates (overlain on B). The precipitates can be observed using TEM (C,D) as dark (electron dense) grains. At high resolution, note the complex spatial relationship between the cyanobacterium filament, encapsulating exopolymer, and (electron dense) minerals. Note, the labelled box in C corresponds to the region shown in D.

Table 1. Reflections and associated lattice spacings measured for the mineral in Figure 4C,D compared to those for hydromagnesite (ICDD, 1975). The numbering of the diffraction spots refers to the numbers on the SAED pattern in 4D.

Diffraction spots in		Hydromagnesite lattice	Measured lattice
Figure 4D	Reflection h k l	spacing (Å)	spacing (Å)
1	3 1 0	2.899000	2.89
2	3 2 1	2.692000	2.69
3	0 2 3	2.207000	2.22
4	5 1 2	1.968000	1.98

## References

- Altermann, W., 2008. Accretion, trapping and binding of sediment in Archean stromatolites—Morphological expression of the antiquity of life. *Space Science Reviews*, 135(1): 55-79.
- Ansari, S., Fatma, T., 2016. Cyanobacterial polyhydroxybutyrate (PHB): Screening, optimization and characterization. *PLoS ONE*, 11(6): e0158168.
- Beck, C., Knoop, H., Axmann, I.M., Steuer, R., 2012. The diversity of cyanobacterial metabolism: Genome analysis of multiple phototrophic microorganisms. *BMC Genomics*, 13: 56.
- Benzerara, K., Menguy, N., López-García, P., Yoon, T.-H., Kazmierczak, J., Tyliczszak, T., Guyot, F., Brown, G.E., 2006. Nanoscale detection of organic signatures in carbonate microbialites. *Proceedings of the National Academy of Sciences*, 103(25): 9440-9445.
- Benzerara, K., Skouri-Panet, F., Li, J., Ferard, C., Gugger, M., Laurent, T., Couradeau, E., Ragon, M., Cosmidis, J., Menguy, N., Margaret-Oliver, I., Tavera, R., Lopez-Garcia, P., Moreira, D., 2014. Intracellular Ca-carbonate biomineralization is widespread in cyanobacteria. *Proceedings of the National Academy of Sciences of the United States of America*, 111(30): 10933-10938.
- Benzerara, K., Yoon, T.H., Tyliczszak, T., Constantz, B., Spormann, A.M., Brown, G.E., 2004. Scanning transmission X-ray microscopy study of microbial calcification. *Geobiology*, 2(4): 249-259.
- Beveridge, T.J., 2006. Visualizing bacterial cell walls and biofilms. *Microbe*, 1(6): 279-284.
- Beveridge, T.J., Graham, L.L., 1991. Surface layers of bacteria. *Microbiological Reviews*, 55(4): 684-705.
- Beveridge, T.J., Murray, R.G., 1976. Uptake and retention of metals by cell walls of *Bacillus subtilis*. *Journal of Bacteriology*, 127(3): 1502-1518.

- Boon, M.E., Kok, L.P., Ouwerkerk-Noordam, E., 1986. Microwave-stimulated diffusion for fast processing of tissue: Reduced dehydrating, clearing, and impregnating times. *Histopathology*, 10(3): 303-309.
- Braissant, O., Decho, A.W., Dupraz, C., Glunk, C., Przekop, K.M., Visscher, P.T., 2007. Exopolymeric substances of sulfate-reducing bacteria: Interactions with calcium at alkaline pH and implication for formation of carbonate minerals. *Geobiology*, 5: 401-411.
- Braissant, O., Decho, A.W., Przekop, K.M., Gallagher, K.L., Glunk, C., Dupraz, C., Visscher, P.T., 2009. Characteristics and turnover of exopolymeric substances in a hypersaline microbial mat. *FEMS Microbiology Ecology*, 67(2): 293-307.
- Burne, R.V., Moore, L.S., 1987. Microbialites: Organosedimentary deposits of benthic microbial communities. *PALAIOS*, 2(3): 241-254.
- Cam, N., Benzerara, K., Georgelin, T., Jaber, M., Lambert, J.-F., Poinot, M., Skouri-Panet, F., Cordier, L., 2016. Selective uptake of alkaline earth metals by cyanobacteria forming intracellular carbonates. *Environmental Science & Technology*, 50(21): 11654-11662.
- Cam, N., Benzerara, K., Georgelin, T., Jaber, M., Lambert, J.F., Poinot, M., Skouri-Panet, F., Moreira, D., Lopez-Garcia, P., Raimbault, E., Cordier, L., Jezequel, D., 2018. Cyanobacterial formation of intracellular Ca-carbonates in undersaturated solutions. *Geobiology*, 16(1): 49-61.
- Damrow, R., Maldener, I., Zilliges, Y., 2016. The multiple functions of common microbial carbon polymers, glycogen and PHB, during stress responses in the non-diazotrophic cyanobacterium *Synechocystis* sp. PCC 6803. *Front Microbiol*, 7: 966.

- de Beer, D., Stoodley, P., Roe, F., Lewandowski, Z., 1994. Effects of biofilm structures on oxygen distribution and mass transport. *Biotechnology and Bioengineering*, 43(11): 1131-8.
- Decho, A.W., Visscher, P.T., Reid, R.P., 2005. Production and cycling of natural microbial exopolymers (EPS) within a marine stromatolite. *Palaeogeography, Palaeoclimatology, Palaeoecology*, 219(1–2): 71-86.
- Dohnalkova, A.C., Marshall, M.J., Arey, B.W., Williams, K.H., Buck, E.C., Fredrickson, J.K., 2011. Imaging hydrated microbial extracellular polymers: Comparative analysis by electron microscopy. *Applied and Environmental Microbiology*, 77(4): 1254-1262.
- Dupraz, C., Reid, R.P., Braissant, O., Decho, A.W., S., N.R., Visscher, L.K., 2009. Processes of carbonate precipitation in modern microbial mats. *Earth-Science Reviews*, 96: 141-162.
- Dupraz, C., Visscher, P.T., 2005. Microbial lithification in marine stromatolites and hypersaline mats. *Trends in Microbiology*, 13: 429-438.
- Dupraz, C., Visscher, P.T., Baumgartner, L.K., Reid, R.P., 2004. Microbe-mineral interactions: Early carbonate precipitation in a hypersaline lake (Eleuthera Island, Bahamas). *Sedimentology*, 51: 745-765.
- Ehrlich, H.L., 1998. Geomicrobiology: Its significance for geology. *Earth-Science Reviews*, 45(1–2): 45-60.
- Ehrlich, H.L., 1999. Microbes as Geologic agents: Their role in mineral formation. *Geomicrobiology Journal*, 16(2): 135-153.
- Fassel, T.A., Mozdziak, P.E., Sanger, J.R., Edmiston, C.E., 1998. Superior preservation of the staphylococcal glycocalyx with aldehyde-ruthenium red and select lysine salts using extended fixation times. *Microsc Res Tech*, 41(4): 291-7.

- Flemming, H.-C., Wingender, J., 2010. The biofilm matrix. *Nature Reviews Microbiology*, 8(9): 623-633.
- Fortin, D., Langley, S., 2005. Formation and occurrence of biogenic iron-rich minerals. *Earth-Science Reviews*, 72(1–2): 1-19.
- Frølund, B., Palmgren, R., Keiding, K., Nielsen, P.H., 1996. Extraction of extracellular polymers from activated sludge using a cation exchange resin. *Water Research*, 30(8): 1749-1758.
- Gallagher, K., Kading, T.J., Braissant, O., Dupraz, C., Visscher, P.T., 2012. Inside the alkalinity engine: The role of electron donors in the organomineralization potential of sulfate-reducing bacteria. *Geobiology*, 10: 518-530.
- Garland, J., Archibald, A., Baddiley, J., 1975. An electron microscopic study of the location of teichoic acid and its contribution to staining reactions in walls of *Streptococcus faecalis* 8191. *Microbiology*, 89(1): 73-86.
- Geesey, G.G., Borch, T., Reardon, C.L., 2008. Resolving biogeochemical phenomena at high spatial resolution through electron microscopy. *Geobiology*, 6(3): 263-269.
- Gillies, A.R., Bushong, E.A., Deerinck, T.J., Ellisman, M.H., Lieber, R.L., 2014. Three-dimensional reconstruction of skeletal muscle extracellular matrix ultrastructure. *Microscopy and Microanalysis*, 20(6): 1835-1840.
- Glud, R.N., Ramsing, N.B., Revsbech, N.P., 1992. Photosynthesis and photosynthesis-coupled respiration in natural biofilms quantified with oxygen microsensors. *Journal of Phycology*, 28(1): 51-60.
- Graham, L.L., Beveridge, T.J., 1990a. Effect of chemical fixatives on accurate preservation of *Escherichia coli* and *Bacillus subtilis* structure in cells prepared by freeze-substitution. *Journal of Bacteriology*, 172(4): 2150-9.

- Graham, L.L., Beveridge, T.J., 1990b. Evaluation of freeze-substitution and conventional embedding protocols for routine electron microscopic processing of eubacteria. *Journal of Bacteriology*, 172(4): 2141-9.
- Graham, L.L., Harris, R., Villiger, W., Beveridge, T.J., 1991. Freeze-substitution of gram-negative eubacteria: General cell morphology and envelope profiles. *Journal of Bacteriology*, 173(5): 1623-1633.
- Haley, M.J., Lawrence, C.B., 2016. The blood–brain barrier after stroke: Structural studies and the role of transcytotic vesicles. *Journal of Cerebral Blood Flow & Metabolism*.
- Hoiczky, E., Baumeister, W., 1995. Envelope structure of four gliding filamentous cyanobacteria. *Journal of Bacteriology*, 177(9): 2387-95.
- Holcomb, P.S., Hoffpauir, B.K., Hoyson, M.C., Jackson, D.R., Deerinck, T.J., Marrs, G.S., Dehoff, M., Wu, J., Ellisman, M.H., Spirou, G.A., 2013. Synaptic inputs compete during rapid formation of the calyx of Held: A new model system for neural development. *The Journal of Neuroscience*, 33(32): 12954-12969.
- ICDD, 1975. International Centre for Diffraction Data, Hydromagnesite card: 00-025-0513, pp. 1.
- Jørgensen, B.B., Des Marais, D.J., 1986. Competition for sulfide among colorless and purple sulfur bacteria in cyanobacterial mats. *FEMS Microbiology Letters*, 38(3): 179-186.
- Jørgensen, B.B., Revsbech, N.P., Blackburn, T.H., Cohen, Y., 1979. Diurnal cycle of oxygen and sulfide microgradients and microbial photosynthesis in a cyanobacterial mat sediment. *Applied and Environmental Microbiology*, 38(1): 46-58.
- Kappler, A., Newman, D.K., 2004. Formation of Fe(III)-minerals by Fe(II)-oxidizing photoautotrophic bacteria. *Geochimica et Cosmochimica Acta*, 68(6): 1217-1226.

- Kittelmann, M., Hawes, C., Hughes, L., 2016. Serial block face scanning electron microscopy and the reconstruction of plant cell membrane systems. *Journal of Microscopy*, 263(2): 200-211.
- Komeili, A., Vali, H., Beveridge, T.J., Newman, D.K., 2004. Magnetosome vesicles are present before magnetite formation, and MamA is required for their activation. *Proceedings of the National Academy of Sciences of the United States of America*, 101(11): 3839-3844.
- Konhauser, K., Ferris, F., 1996. Diversity of iron and silica precipitation by microbial mats in hydrothermal waters, Iceland: Implications for Precambrian iron formations. *Geology*, 24(4): 323-326.
- Körstgens, V., Flemming, H.-C., Wingender, J., Borchard, W., 2001. Influence of calcium ions on the mechanical properties of a model biofilm of mucoid *Pseudomonas aeruginosa*. *Water Science and Technology*, 43(6): 49-57.
- Langley, S., Gault, A., Ibrahim, A., Renaud, R., Fortin, D., Clark, I.D., Ferris, F.G., 2009. A comparison of the rates of Fe(III) reduction in synthetic and bacteriogenic iron oxides by *Shewanella putrefaciens* CN32. *Geomicrobiology Journal*, 26(2): 57-70.
- Lawrence, J.R., Swerhone, G.D.W., Leppard, G.G., Araki, T., Zhang, X., West, M.M., Hitchcock, A.P., 2003. Scanning transmission X-ray, laser scanning, and transmission electron microscopy mapping of the exopolymeric matrix of microbial biofilms. *Applied and Environmental Microbiology*, 69(9): 5543-5554.
- Li, J., Margaret Oliver, I., Cam, N., Boudier, T., Blondeau, M., Leroy, E., Cosmidis, J., Skouri-Panet, F., Guigner, J.-M., Féraud, C., Poinot, M., Moreira, D., Lopez-Garcia, P., Cassier-Chauvat, C., Chauvat, F., Benzerara, K., 2016. Biomineralization Patterns of Intracellular Carbonatogenesis in Cyanobacteria: Molecular Hypotheses. *Minerals*, 6(1): 10.

- Luft, J.H., 1961. Improvements in epoxy resin embedding methods. *J Biophys Biochem Cytol*, 9: 409-14.
- Madison, L.L., Huisman, G.W., 1999. Metabolic engineering of poly(3-hydroxyalkanoates): From DNA to plastic. *Microbiology and Molecular Biology Reviews*, 63(1): 21-53.
- McCutcheon, J., Nothdurft, L., Webb, G.E., Paterson, D., Southam, G., 2016a. Beachrock formation via microbial dissolution and re-precipitation of carbonate minerals. *Marine Geology*, 382: 122-135.
- McCutcheon, J., Nothdurft, L.D., Webb, G.E., Shuster, J., Nothdurft, L., Paterson, D., Southam, G., 2017a. Building biogenic beachrock: Visualizing microbially-mediated carbonate cement precipitation using XFM and a strontium tracer. *Chemical Geology*, 465: 21-34.
- McCutcheon, J., Power, I.M., Harrison, A.L., Dipple, G.M., Southam, G., 2014. A greenhouse-scale photosynthetic microbial bioreactor for carbon sequestration in magnesium carbonate minerals. *Environmental Science & Technology*, 48(16): 9142-9151.
- McCutcheon, J., Turvey, C.C., Wilson, S.A., Hamilton, J.L., Southam, G., 2017b. Experimental deployment of microbial mineral carbonation at an asbestos mine: Potential applications to carbon storage and tailings stabilization. *Minerals*, 7: 191.
- McCutcheon, J., Wilson, S.A., Southam, G., 2016b. Microbially accelerated carbonate mineral precipitation as a strategy for in situ carbon sequestration and rehabilitation of asbestos mine sites. *Environmental Science & Technology*, 50(3): 1419-1427.
- McDonald, K., 1984. Osmium ferricyanide fixation improves microfilament preservation and membrane visualization in a variety of animal cell types. *Journal of Ultrastructure Research*, 86(2): 107-118.

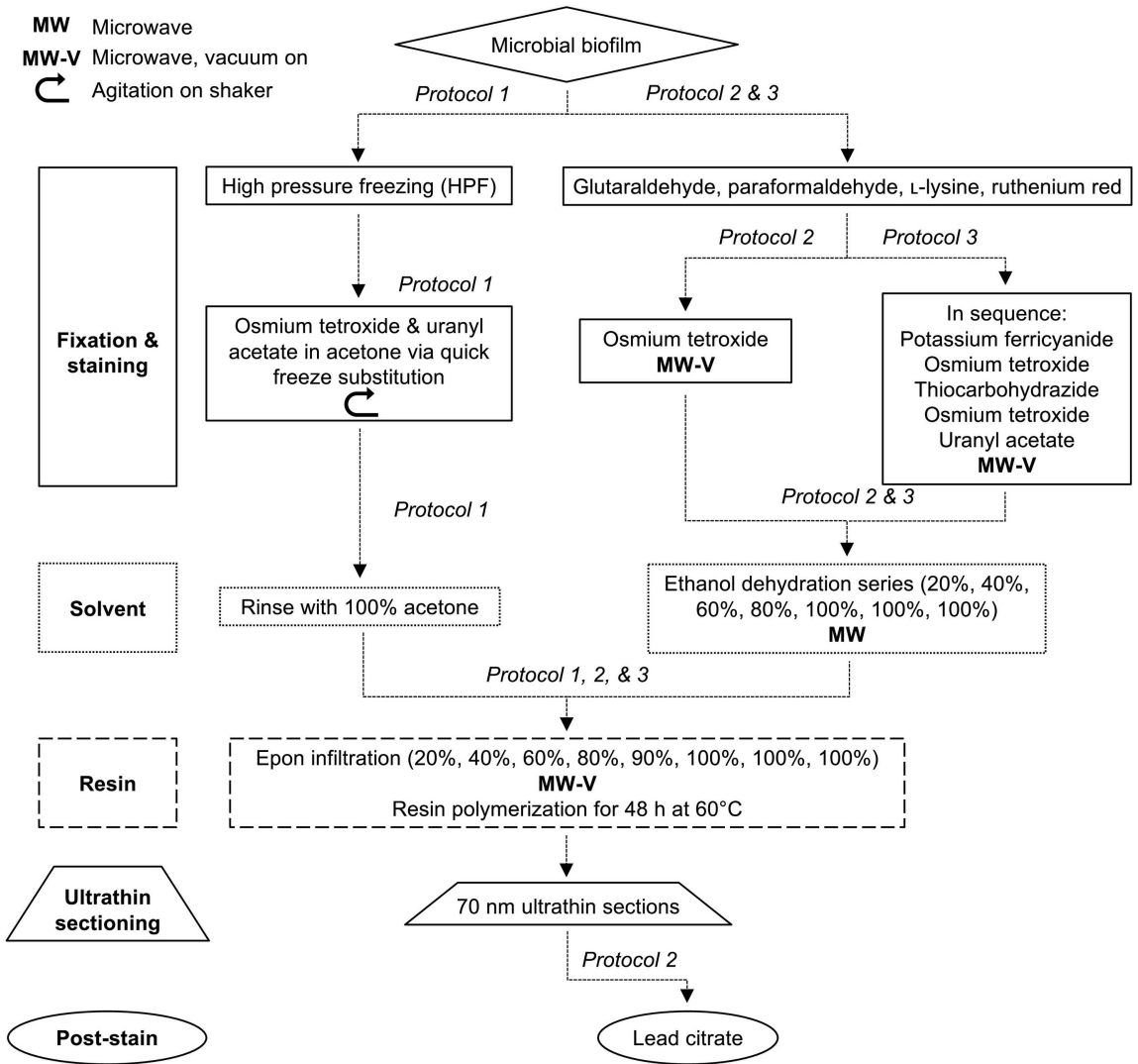
- McDonald, K., 1999. High-pressure freezing for preservation of high resolution fine structure and antigenicity for immunolabeling. In: Nasser Hajibagheri, M.A. (Ed.), *Electron Microscopy Methods and Protocols*. Humana Press, Totowa, NJ, pp. 77-97.
- McDonald, K., 2007. Cryopreparation Methods for Electron Microscopy of Selected Model Systems, *Methods in Cell Biology*. Academic Press, pp. 23-56.
- McDonald, K.L., 2014. Out with the old and in with the new: Rapid specimen preparation procedures for electron microscopy of sectioned biological material. *Protoplasma*, 251(2): 429-448.
- McDonald, K.L., Webb, R.I., 2011. Freeze substitution in 3 hours or less. *Journal of Microscopy*, 243(3): 227-233.
- Mehta, K.K., Evitt, N.H., Swartz, J.R., 2015. Chemical lysis of cyanobacteria. *Journal of Biological Engineering*, 9: 10.
- Miot, J., Benzerara, K., Kappler, A., 2014. Investigating microbe-mineral interactions: Recent advances in X-ray and electron microscopy and redox-sensitive methods. *Annual Review of Earth and Planetary Sciences*, 42(1): 271-289.
- Miot, J., Maclellan, K., Benzerara, K., Boisset, N., 2011. Preservation of protein globules and peptidoglycan in the mineralized cell wall of nitrate-reducing, iron(II)-oxidizing bacteria: a cryo-electron microscopy study. *Geobiology*, 9(6): 459-470.
- Mouw, J.K., Ou, G., Weaver, V.M., 2014. Extracellular matrix assembly: A multiscale deconstruction. *Nature Reviews Molecular Cell Biology*, 15(12): 771-785.
- Obst, M., Dittrich, M., 2005. Living under an atomic force microscope: An optimized approach for in vivo investigations on surface alterations towards biomineral nucleation on cyanobacterial cells. *Geobiology*, 5: 179-193.
- Pace, A., Bourillot, R., Bouton, A., Vennin, E., Braissant, O., Dupraz, C., Duteil, T., Bundeleva, I., Patrier, P., Galaup, S., Yokoyama, Y., Franceschi, M., Virgone, A.,

- Visscher, P.T., 2018. Formation of stromatolite lamina at the interface of oxygenic–anoxygenic photosynthesis. *Geobiology*, 0: 1-21.
- Palade, G.E., 1952. A study of fixation for electron microscopy. *The Journal of Experimental Medicine*, 95(3): 285-98.
- Phoenix, V.R., Konhauser, K.O., 2008. Benefits of bacterial biomineralization. *Geobiology*, 6(3): 303-8.
- Potts, M., 1994. Desiccation tolerance of prokaryotes. *Microbiological Reviews*, 58(4): 755-805.
- Rae, B.D., Long, B.M., Badger, M.R., Price, G.D., 2013. Functions, compositions, and evolution of the two types of carboxysomes: Polyhedral microcompartments that facilitate CO<sub>2</sub> fixation in cyanobacteria and some proteobacteria. *Microbiology and Molecular Biology Reviews*, 77(3): 357-379.
- Randles, M.J., Collinson, S., Starborg, T., Mironov, A., Krendel, M., Königshausen, E., Sellin, L., Roberts, I.S.D., Kadler, K.E., Miner, J.H., Lennon, R., 2016. Three-dimensional electron microscopy reveals the evolution of glomerular barrier injury. *Scientific Reports*, 6: 35068.
- Reid, R.P., Visscher, P.T., Decho, A.W., Stolz, J.F., Bebout, B.M., Dupraz, C., Macintyre, I.G., Paerl, H.W., Pinckney, J.L., Prufert-Bebout, L., Steppe, T.F., DesMarais, D.J., 2000. The role of microbes in accretion, lamination and early lithification of modern marine stromatolites. *Nature*, 406: 989.
- Reusch, R.N., 2012. Physiological importance of poly-(R)-3-hydroxybutyrates. *Chem Biodivers*, 9(11): 2343-66.
- Reusch, R.N., Sadoff, H.L., 1988. Putative structure and functions of a poly-beta-hydroxybutyrate/calcium polyphosphate channel in bacterial plasma membranes.

- Proceedings of the National Academy of Sciences of the United States of America, 85(12): 4176-4180.
- Reynolds, E.S., 1963. The use of lead citrate at high pH as an electron-opaque stain in electron microscopy. *The Journal of Cell Biology*, 17(1): 208-212.
- Riding, R., 2000. Microbial carbonates: the geological record of calcified bacterial-algal mats and biofilms. *Sedimentology*, 47: 179-214.
- Roberson, E.B., Firestone, M.K., 1992. Relationship between desiccation and exopolysaccharide production in a soil *Pseudomonas* sp. *Applied and Environmental Microbiology*, 58(4): 1284-1291.
- Seligman, A.M., Wasserkrug, H.L., Hanker, J.S., 1966. A new staining method (OTO) for enhancing contrast of lipid-containing membranes and droplets in osmium tetroxide-fixed tissue with osmiophilic thiocarbonylhydrazide (TCH). *The Journal of Cell Biology*, 30(2): 424-432.
- Shuster, J., Marsden, S., Maclean, L.C.W., Ball, J., Bolin, T., Southam, G., 2015. The immobilization of gold from gold (III) chloride by a halophilic sulphate-reducing bacterial consortium. *Geological Society, London, Special Publications*, 393(1): 249-263.
- Southam, G., 2012. Minerals as substrates for life: The Prokaryotic view. *Elements*, 8(2): 101-106.
- Southam, G., Beveridge, T.J., 1994. The in vitro formation of placer gold by bacteria. *Geochimica et Cosmochimica Acta*, 58(20): 4527-4530.
- Southam, G., Firtel, M., Blackford, B.L., Jericho, M.H., Xu, W., Mulhern, P.J., Beveridge, T.J., 1993. Transmission electron microscopy, scanning tunneling microscopy, and atomic force microscopy of the cell envelope layers of the archaeobacterium *Methanospirillum hungatei* GP1. *Journal of Bacteriology*, 175(7): 1946-1955.

- Starborg, T., Kadler, K.E., 2015. Serial block face-scanning electron microscopy: A tool for studying embryonic development at the cell–matrix interface. *Birth Defects Research Part C: Embryo Today: Reviews*, 105(1): 9-18.
- Starborg, T., Kalson, N.S., Lu, Y., Mironov, A., Cootes, T.F., Holmes, D.F., Kadler, K.E., 2013. Using transmission electron microscopy and 3View to determine collagen fibril size and three-dimensional organization. *Nat. Protocols*, 8(7): 1433-1448.
- Stewart, P.S., Franklin, M.J., 2008. Physiological heterogeneity in biofilms. *Nature Reviews Microbiology*, 6(3): 199-210.
- Visscher, P.T., Stolz, J.F., 2005. Microbial mats as bioreactors: Populations, processes, and products. *Palaeogeography, Palaeoclimatology, Palaeoecology*, 219(1–2): 87-100.
- Vonshak, A., 1986. Laboratory techniques for the cultivation of microalgae. In: Richmond, A. (Ed.), *CRC handbook of microalgae mass culture*. CRC Press Inc., Boca Raton, pp. 117.
- Watson, M.L., 1958. Staining of tissue sections for electron microscopy with heavy metals. *The Journal of Biophysical and Biochemical Cytology*, 4(4): 475-478.
- Webb, G.E., Jell, J.S., Baker, J.C., 1999. Cryptic intertidal microbialites in beachrock, Heron Island, Great Barrier Reef: implications for the origin of microcrystalline beachrock cement. *Sedimentary Geology*, 126(1-4): 317-334.
- Yamauchi, Y., Kaniya, Y., Kaneko, Y., Hihara, Y., 2011. Physiological roles of the cyAbrB transcriptional regulator pair Sll0822 and Sll0359 in *Synechocystis* sp. strain PCC 6803. *Journal of Bacteriology*, 193(15): 3702-3709.
- Young, R.D., Knupp, C., Pinali, C., Png, K.M.Y., Ralphs, J.R., Bushby, A.J., Starborg, T., Kadler, K.E., Quantock, A.J., 2014. Three-dimensional aspects of matrix assembly by cells in the developing cornea. *Proceedings of the National Academy of Sciences*, 111(2): 687-692.

- Yu, J., Liberton, M., Cliften, P.F., Head, R.D., Jacobs, J.M., Smith, R.D., Koppenaal, D.W., Brand, J.J., Pakrasi, H.B., 2015. *Synechococcus elongatus* UTEX 2973, a fast growing cyanobacterial chassis for biosynthesis using light and CO<sub>2</sub>. *Scientific Reports*, 5: 8132.
- Zhang, X., Sherman, D.M., Sherman, L.A., 2014. The uptake hydrogenase in the unicellular diazotrophic cyanobacterium *Cyanothece* sp. strain PCC 7822 protects nitrogenase from oxygen toxicity. *Journal of Bacteriology*, 196(4): 840-849.



Protocol	Useful references
L-lysine and ruthenium-red	Fassel, et al., 1998
Potassium ferricyanide	McDonald, 1984
Uranyl acetate	Watson, 1958; McDonald, 1984
Osmium tetroxide	Palade, 1952
Osmium tetroxide-thiocarbohydrazide-osmium tetroxide	Seligman, Wasserkrug, & Hanker, 1966
EPON Embed 812 resin	Luft, 1961
Reynolds' lead citrate post-stain	Reynolds, 1963
Brain tissue 3D reconstruction staining protocol	Holcomb et al., 2013
Quick freeze substitution	McDonald & Webb, 2011, McDonald, 2014

Figure 1

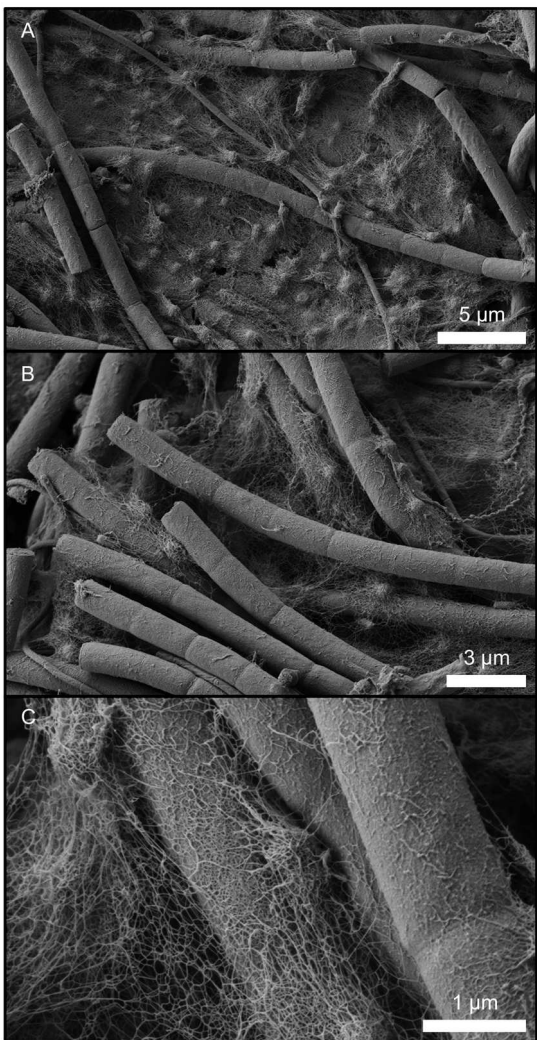


Figure 2

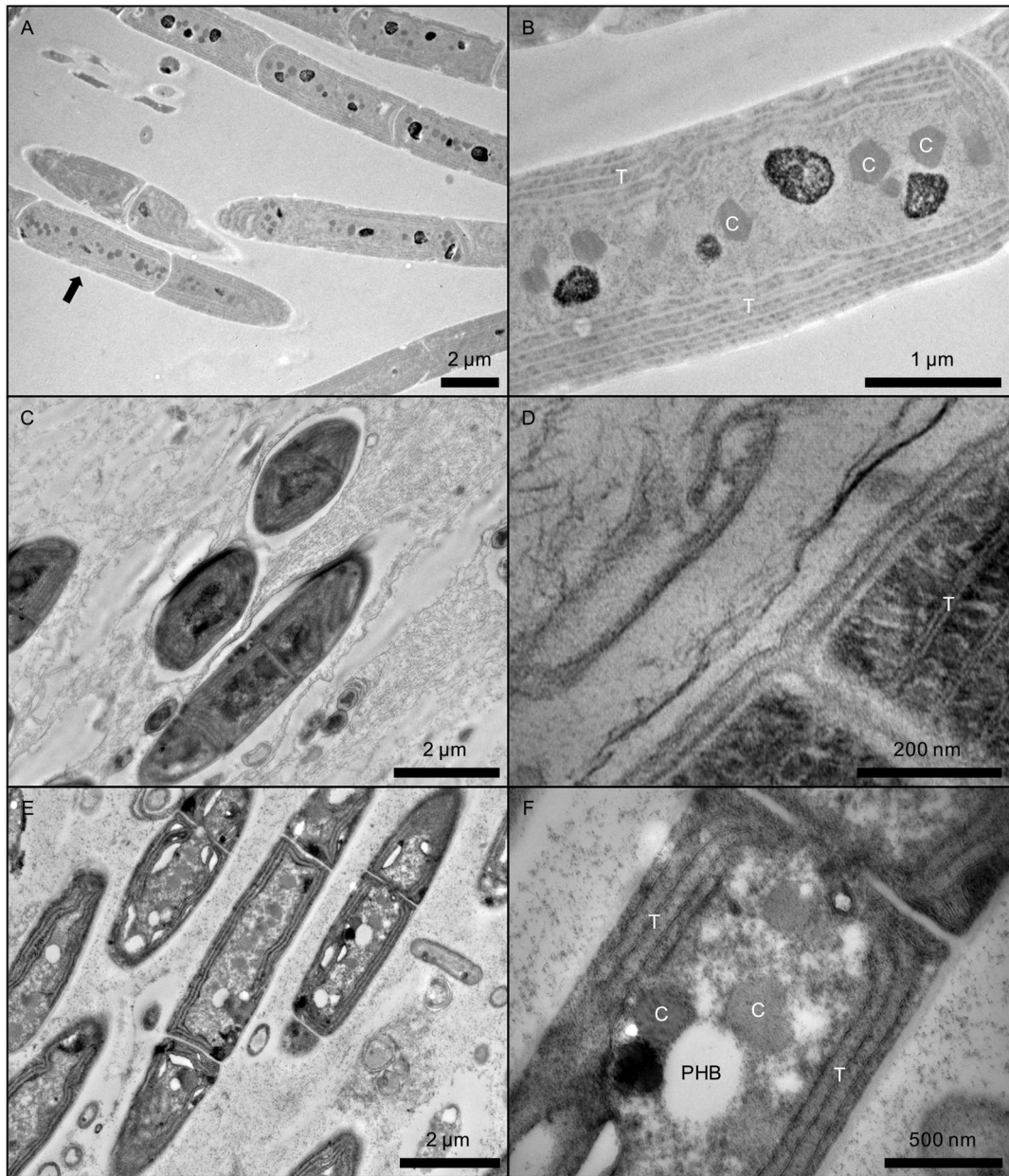


Figure 3

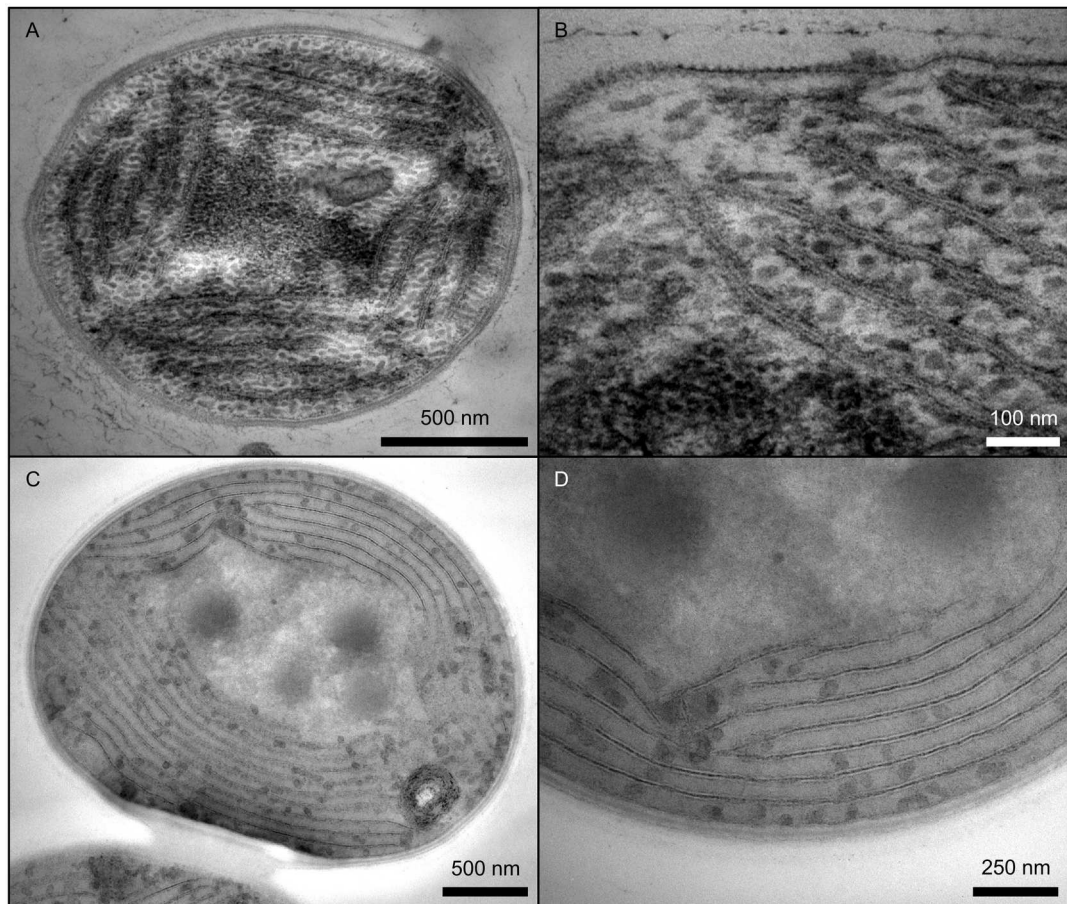


Figure 4

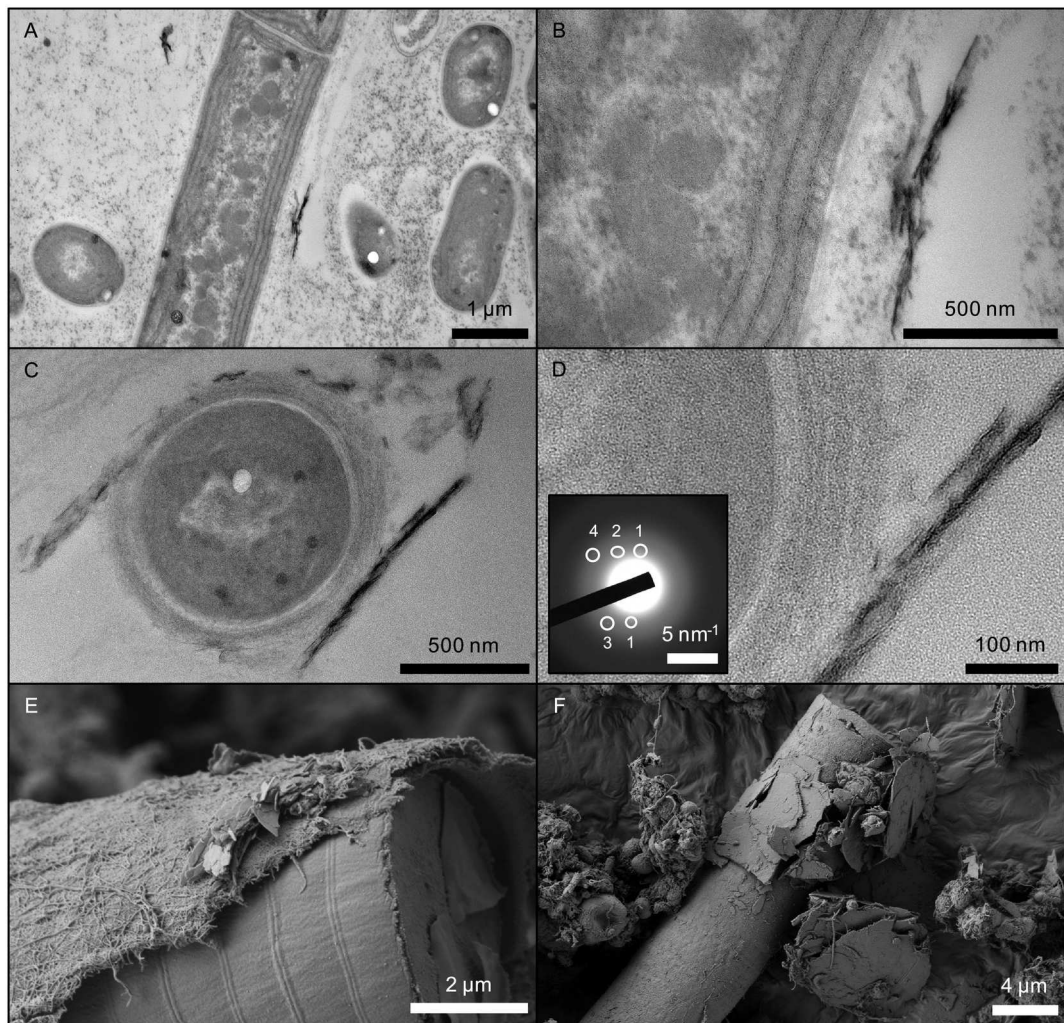


Figure 5

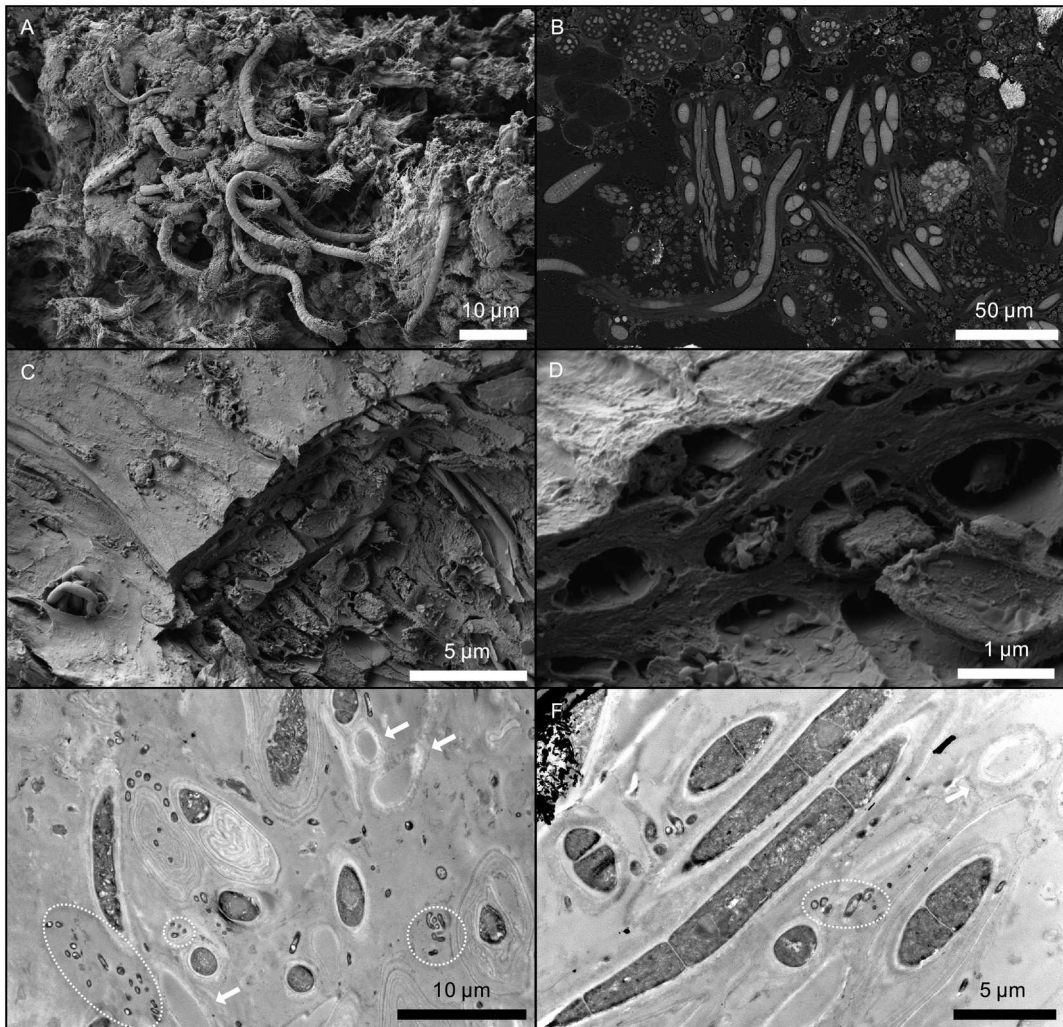


Figure 6

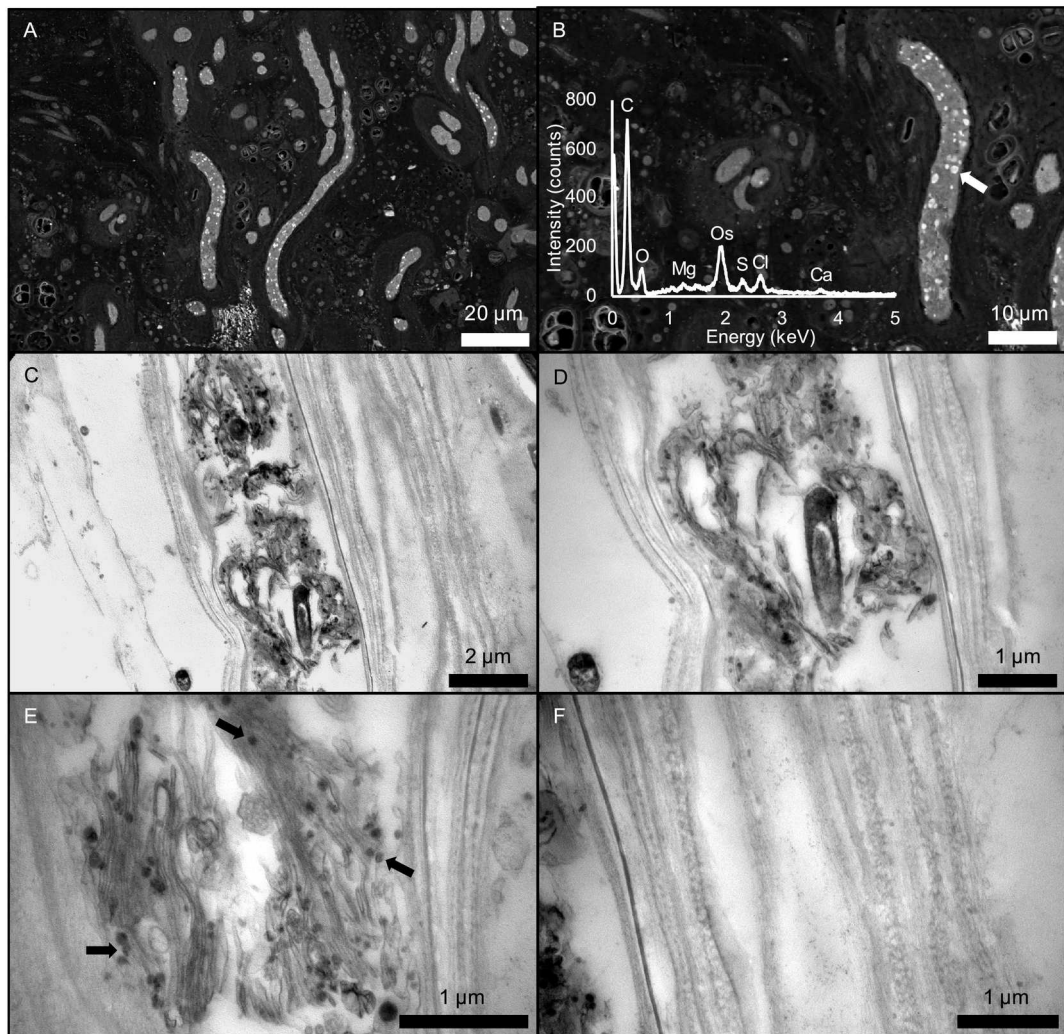


Figure 7

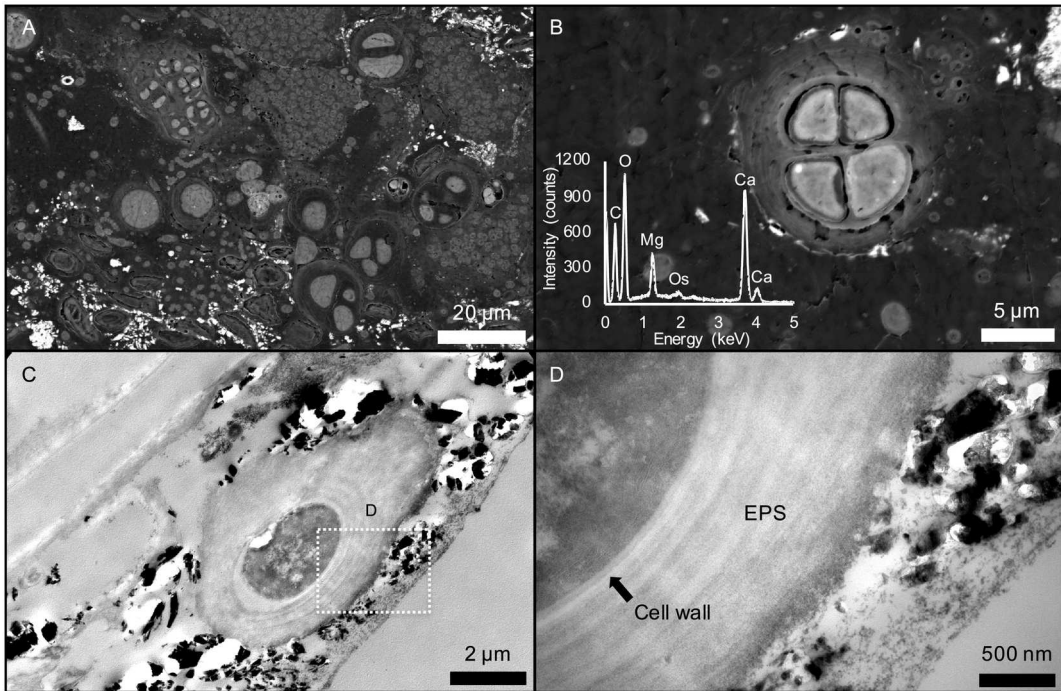


Figure 8